Molecular dynamics of model liquid crystals composed of semiflexible molecules

Frédéric Affouard, Martin Kröger,* and Siegfried Hess
Institut für Theoretische Physik, Technische Universität Berlin, Hardenbergstrasse 36, D-10623 Berlin, Germany
(Received 6 March 1996)

Results of molecular-dynamics computer simulations are presented for a simple microscopic model of thermotropic liquid crystals. The system is composed of short multibead semiflexible chains where the beads are connected by an anharmonic spring. The intermolecular bead-bead interactions are modeled by Lennard-Jones potentials, the attractive part is taken into account only between the stiff parts. Heating the system, solid, smectic-*A*, and liquid phases are found. For the symmetric molecules and anisotropic potentials studied first, the smectic-*A* phase is clearly defined over a wide range of temperatures, whereas the nematic phase is not present or too narrow in temperature to be seen clearly. The evolution of the systems has also been studied as a function of the length of flexible parts and the strength of the stiff-stiff potential. [S1063-651X(96)00211-5]

PACS number(s): 61.30.Cz, 02.70.Ns, 64.70.Md

I. INTRODUCTION

Thermotropic liquid crystals form mesophases intermediate between a solid phase at low temperatures and an isotropic liquid phase at high temperatures [1–3]. Nematic liquid crystals possess an orientational order of the molecular axes, but no long-range positional order, complementary to plastic crystals, which have a crystal-like positional order, but a dynamical orientational disorder [4,5]. Smectic liquid crystals, in particular those referred to as Sm-*A* and Sm-*C*, have a nematiclike orientational order and in addition their centers of mass are confined to layers. Computational studies of the material properties of complex fluids by molecular dynamics (MD) are feasible and desirable for models that, on the one hand, are simple enough to allow efficient simulations and, on the other hand, catch those features that are typical for the intermolecular interactions.

Previous computational studies on the phase behavior of model liquid crystals by MD and Monte Carlo simulations have been performed on various levels of simplification of the molecular interactions [6,7]. The first atomistic simulations of the nematic phase of 4-*n*-pentyl-4′-cyanobiphenyl (5CB) compounds [8], the smectic multibilayer [9,10], and discotic phases [11] were still too limited in the size of the systems and the durations of the runs. Simulations of the Lebwohl-Lasher lattice model [12,13] gave hints of the basic features of the phase transitions. The simplest approach where the dynamics of the centers of mass of the particles are properly taken into account is to treat molecules as stiff nonspherical particles such as ellipsoids or spherocylinders or to consider particles interacting by a Gay-Berne potential [14–16]. Going further, the internal configuration has been taken into account by treating the molecules as being composed of interaction sites (monomers) connected by formulating constraints or binding forces. Both Monte Carlo [9,17–19] and molecular-dynamics methods [20–22] were applied to study the static and dynamic properties, respectively. With the advent of new generations of supercomputers, modern workstations, and new techniques [23], simulations of complex real systems are now possible showing good agreement with the experimental results [24], such as for the nematic phase of 5CB [25,26] or the smectic-*C* phase of *p*-(*n*-decyloxybenzylidene)-*p*-amino-2-methylbutylcinnamate [21] at moderate time and length scales. Allen [27] recently simulated extremely huge compounds such as lipids in the liquid-crystalline phase [28]. However, from a physical point of view the construction of model interactions remains in question and from a technical point of view the development of efficient parallel codes [29–31] becomes more and more difficult due the complexity of the models that involve long-range electrostatic forces or many-body potentials.

To overcome parts of these problems, to extend former models, and to study bulk properties of liquid crystals in this work we consider a model fluid composed of partially stiff and partially flexible molecules as they occur in most real thermotropic liquid crystals (cf. Fig. 1). The model is analyzed by applying the molecular-dynamics method in order to provide complete information about the phase-space dynamics. Precisely, our model system is composed of a number of short chains where ten (or eleven) monomers (beads) are connected by finitely extendable nonlinear elastic (FENE) springs, an approach that is of use in simulations of polymeric liquids [32,33]. For each molecule, the central part (four or five beads) is stiff, while both terminals are flexible. The lengths of both stiff and flexible parts are parameters of the model. The intermolecular bead-bead interactions are Lennard-Jones (LJ) potentials, whose attractive part is taken into account only between the monomers in stiff parts. The strength of the attractive part is controlled by a parameter ϵ_{att}. For the particular model parameters used first, a phase transition Sm-*A*–isotropic liquid was found both by heating and cooling the sample. Although the absence of an intermediate nematic phase seems to be surprising at first glance, a number of liquid-crystalline compounds do have such a phase behavior. Before material properties such as diffusion, elasticity, or viscosity coefficients are computed, the phase behavior of the system under investigation is to be determined. For comparison with the simulations of [34], some

*Author to whom correspondence should be addressed. Electronic address: mk@polly.physik.tu-berlin.de

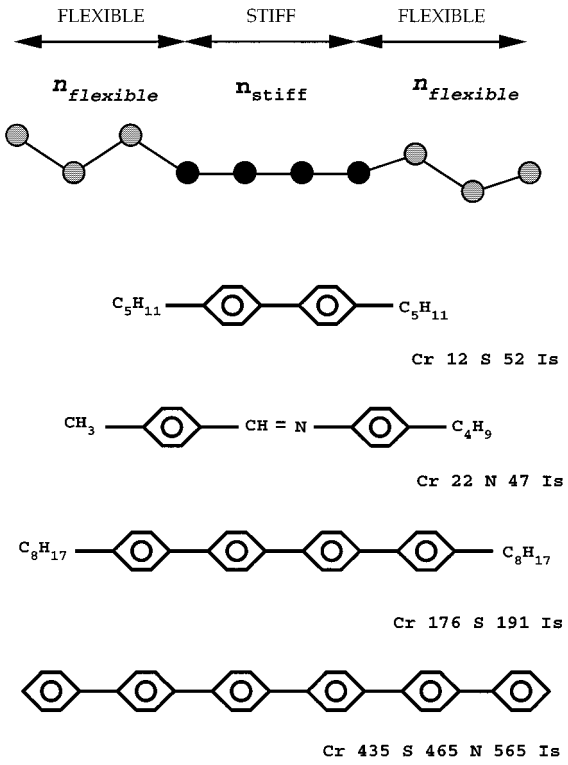

FIG. 1. Comparison between a modeled chain with stiff and flexible parts ($n_{\rm flex}$-$n_{\rm stiff}$-$n_{\rm flex}$) and real compounds that present nematic and/or smectic phases.

calculations for stiff chains without flexible ends are also performed.

This paper is organized as follows. In Sec. II the model for semiflexible liquid crystals is presented and details of the simulation are given. Section III contains the results of the simulation for heating and cooling. The influence of the strength of the attractive potential for different lengths of rigid and flexible parts is discussed. Conclusions are given in Sec. IV.

II. MODEL AND DETAILS OF THE SIMULATION

The model system is composed of N_c multibead chains with typically $n_b=10$ beads per chain. Neighboring beads within chains are connected by an anharmonic FENE spring. The potentials are given in Sec. II A. Here each chain, as shown in Fig. 1, is made of two identical terminal flexible parts ($n_{\rm flex}$ beads), and a stiff central stiff part ($n_{\rm stiff}$ beads), where $n_{\rm stiff}+2\times n_{\rm flex}=n_b$.

The notation ($n_{\rm flex}$-$n_{\rm stiff}$-$n_{\rm flex}$) is used here to define the different systems. For example, *3*-4-*3* means that the chains in this system are composed of a central stiff part of four beads and two terminal flexible parts of three beads. The simulations are performed in the NVT statistical ensemble, where the total number of beads ($N=N_c n_b$), the volume (V), and the temperature (T) are fixed. The temperature is kept constant by rescaling all velocities at every time step [35]. The geometry of the system is a parallelepiped box ($L_x=L_y\simeq\frac{1}{3}L_z$) with periodic boundary conditions [36] in order to study bulk properties. Newton's equations of motion for this classical many particles problem are integrated by the Verlet algorithm [37] in a molecular-dynamics computer simulation. Throughout this paper all quantities are expressed in the usual LJ reduced units [35].

We will present results for a system of $N_c=288$ chains of length $n_b=10$ at bead number density $\rho\equiv N/V=0.8$. An initial low temperature solid phase is chosen as a fcc structure ($4\times4\times4$ cells) where all chains are parallel along the z direction. Considering the intramolecular vibrations [38], an integration time step of $\Delta t=0.005$ is used.

A. Model potentials

Two types of potentials are used: a Lennard-Jones potential $U_{\rm LJ}$ (full and truncated versions) and an attractive FENE potential $U_{\rm FENE}$ used previously to study flexible polymers [38,39,33],

$$U_{\rm LJ}^{\rm rep}=\begin{cases}4\,[r^{-12}-r^{-6}+1/4] & \text{for } r\leqslant 2^{1/6}\\ 0 \text{ for } r>2^{1/6}\end{cases} \tag{1}$$

and

$$U_{\rm LJ}^{\rm att}=\begin{cases}-\epsilon_{\rm att} \text{ for } r\leqslant 2^{1/6}\\ 4\epsilon_{\rm att}[r^{-12}-r^{-6}] \text{ for } 2^{1/6}<r\leqslant 2.5\\ 0 \text{ for } r>2.5\,,\end{cases} \tag{2}$$

where r is the distance between two interaction centers (beads), $U_{\rm LJ}^{\rm rep}$ corresponds to a purely repulsive LJ potential, and $U_{\rm LJ}^{\rm att}$ corresponds to a purely attractive LJ potential. The strength of the attractive LJ potential $U_{\rm LJ}^{\rm att}$ is parametrized by $\epsilon_{\rm att}$. The FENE potential is written as

$$U_{\rm FENE}=\begin{cases}-0.5kR_0^2\ln[1-(r/R_0)^2] \text{ for } r\leqslant R_0\\ \infty \text{ for } r>R_0\,,\end{cases} \tag{3}$$

with $R_0=1.5$ and $k=30$ as in [38,33].

The radial symmetric interaction potential $U_{\alpha i,\beta j}^{\rm total}(r)$ for the model fluid between bead i of chain α (coordinates $\mathbf{r}_\alpha^i$) and bead j of chain β, where $i,j\in 1,\ldots,n_b$ and $\alpha,\beta\in 1,\ldots,N_c$, is written as

$$\begin{aligned}U_{\alpha i,\beta j}^{\rm total}(r)&\equiv U_{\rm LJ}^{\rm rep}(r)+\delta_{\alpha,\beta}\;\delta_{1,|i-j|}\;U_{\rm FENE}(r)\\&+\delta_{\alpha,\beta}\;\delta_{i+j,n_b+1}\;\delta_{r_{\rm stiff},|i-j|}\;[U_{\rm LJ}^{\rm rep}+U_{\rm FENE}](r/r_{\rm stiff})\\&+\Theta(n_{\rm stiff}-|2i-n_b-1|)\,\delta_{i,|j+\phi_{\alpha\beta}(n_b+1)|}\\&\times(1-\delta_{\alpha,\beta})\;U_{\rm LJ}^{\rm att}(r)\,,\end{aligned} \tag{4}$$

with $\phi_{\alpha\beta}=0$ and $\phi_{\alpha\beta}=-1$ for ''parallel'' and ''antiparallel'' chains α,β, respectively, which can be written formally as

$$\phi_{\alpha\beta}\equiv\Theta(\mathbf{r}_{\alpha\alpha}^{n_{\rm flex}+1,n_b-n_{\rm flex}}\cdot\mathbf{r}_{\beta\beta}^{n_{\rm flex}+1,n_b-n_{\rm flex}})-1\,. \tag{5}$$

Here $\mathbf{r}_{\alpha\beta}^{ij}=\mathbf{r}_\alpha^i-\mathbf{r}_\beta^j$ is the vector connecting two bead coordinates and the contour length of the stiff part is $r_{\rm stiff}\equiv n_{\rm stiff}-1$. The terms involving the step function Θ with $\Theta(x)=1$ for $x>0$ and $\Theta(x)=0$ for $x\leqslant 0$ in Eqs. (4) and (5)

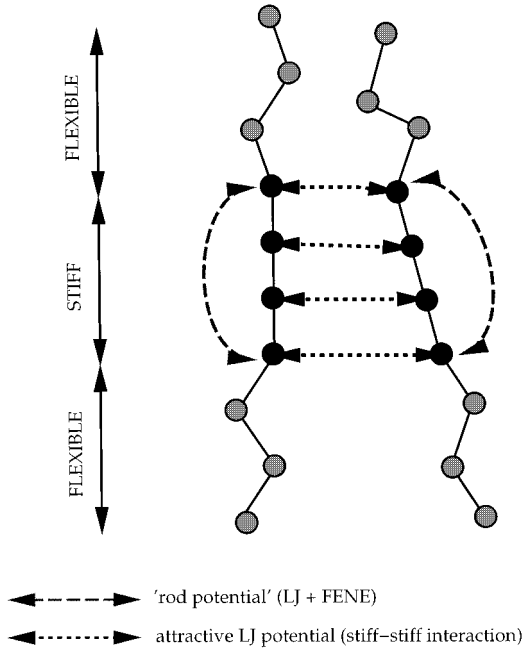

FIG. 2. Bead-bead interactions. In addition to the interactions indicated in this figure, there are also a FENE interaction between all connected beads in chains and a repulsive Lennard-Jones between all beads of the system.

ensure that the labeling of the particles within the chains does not violate the head-tail symmetry. The term $\Theta(n_{\text{stiff}}-|2i-n_b-1|)$ vanishes except for beads within the stiff part, i.e., for $i\in[n_{\text{flex}}+1,n_b-n_{\text{flex}}]$. For pairs of beads i,j of this type on different chains α,β, the Kronecker symbol $\delta_{i,|j+\phi_{\alpha\beta}(n_b+1)|}$ is nonvanishing for $i=j$ (parallel) and $i=n_b-j+1$ (antiparallel chains).

Hence there are four qualitatively different bead-bead interactions in the model written as a combination of the potentials defined in Eqs. (2) and (3). Figure 2 shows interactions in play between two representative chains. According to (4) all beads are interacting with a $U_{\text{LJ}}^{\text{rep}}$ Lennard-Jones potential; directly connected beads in the chain interact with the U_{FENE} attractive potential. The central part of each chain is kept stiff with a weak ''rod potential'' between two terminals of the stiff part; ''corresponding'' beads of stiff parts of different chains interact via the attractive potential $U_{\text{LJ}}^{\text{att}}$, which results in an effectively anisotropic interaction between stiff parts. Its depth can be adjusted by the parameter ϵ_{att}.

B. Characterization of the system

1. Static structure factor

The static structure factor of the model fluid where each bead is assumed to act as a ''scatterer'' is

$$S(\mathbf{k})=\frac{1}{N}\left\langle\left|\sum_{\alpha=1}^{N_c}\sum_{j=1}^{n_b}\exp(i\mathbf{k}\cdot\mathbf{r}_j^{\alpha})\right|^2\right\rangle=S_{\text{SC}}(\mathbf{k})\;S_{\text{inter}}(\mathbf{k}). \tag{6}$$

Here S_{SC} is the single-chain static structure factor representing the intramolecular correlations

$$S_{\text{SC}}(\mathbf{k})=\frac{1}{N}\sum_{\alpha=1}^{N_c}\left\langle\left|\sum_{j=1}^{n_b}\exp(i\mathbf{k}\cdot\mathbf{r}_j^{\alpha})\right|^2\right\rangle, \tag{7}$$

where $\mathbf{r}_j^{\alpha}$ is the position of the bead j of the molecule α, $\mathbf{k}$ the relevant wave vector, and $N=N_c n_b$ the total number of beads [33]. The static structure factor $S(\mathbf{k})$ is restricted to $k=|\mathbf{k}|=p(2\pi/L_x)$ (p an integer) because of the geometry of the system, which is a parallelepiped box ($L_x=L_y\simeq\frac{1}{3}L_z$) with periodic boundary conditions. The single-chain static structure $S_{\text{SC}}(\mathbf{k})$ is not subject to this restriction for k because it can be calculated from the unfolded chains, independent of the size of the basic simulation box.

A long-range positional order could be revealed by Bragg-like peaks in the static structure factor $S_{\text{c.m.}}(\mathbf{k})$, where the centers of mass of the molecules are taken as scatterers. The height of the Bragg peaks approach N_c for a system composed of N_c molecules. Due to the initial preparation of the system, such peaks would show up for wave vectors $\mathbf{k}$ parallel to the z direction. For a system with a layer distance d a peak occurs at $k=2\pi/d$. Its height divided by N_c provides a convenient measure for the degree of positional order. Thus we use the ''positional order parameter'' σ,

$$\sigma=\left|\left\langle\frac{1}{N_c}\sum_{j=1}^{N_c}\exp\left(\frac{2i\pi z_j}{d}\right)\right\rangle\right|, \tag{8}$$

where z_j is the z coordinate of the center of mass of chain j and $\langle\ \rangle$ denotes the average over time. The layer distance d is about the length of the chain and we chose $d=n_b-1$. The detailed calculation of $S_{\text{c.m.}}(\mathbf{k})$ is not made because of the inappropriate resolution of the wave vectors $\mathbf{k}$ compatible with the simulation box. The intramolecular structure factor S_{SC}, which contains information on the distance and the orientations of the beads within a single chain, however, can be computed reliably and examples will be presented.

2. Macroscopic orientational order parameters

We define the direction of the rigid part of a chain as the main symmetry molecular axis **a**. Classically, the macroscopical orientational (Maier-Saupe) order parameter S_2 is computed from the knowledge of all molecular axes **a**. An instantaneous alignment tensor is defined as

$$Q_{\alpha\beta}=\frac{1}{N_c}\sum_{i=1}^{N_c}\frac{3}{2}\left[(\mathbf{a}_i)_\alpha(\mathbf{a}_i)_\beta-\frac{1}{3}\delta_{\alpha\beta}\right], \tag{9}$$

where N_c is the number of chains in the system and $(\mathbf{a}_i)_\alpha$ are the Cartesian coordinates ($\alpha=x,y,z$) of the axis of chain i ($i=1,2,\ldots,N_c$). The time average of the largest eigenvalue of the alignment tensor $Q_{\alpha\beta}$ is equal to the orientational order parameter S_2 and the associated eigenvector gives the macroscopic director **n** [40]. In the case of uniaxial orientational order of molecules the alignment tensor reads $Q_{\alpha\beta}=S_2(n_\alpha n_\beta-\frac{1}{3}\delta_{\alpha\beta})$.

To characterize the flexibility along the chains, we computed the average angles θ_{stiff} and θ_{flex} between two successive segments in flexible and stiff parts, respectively. They are defined as:

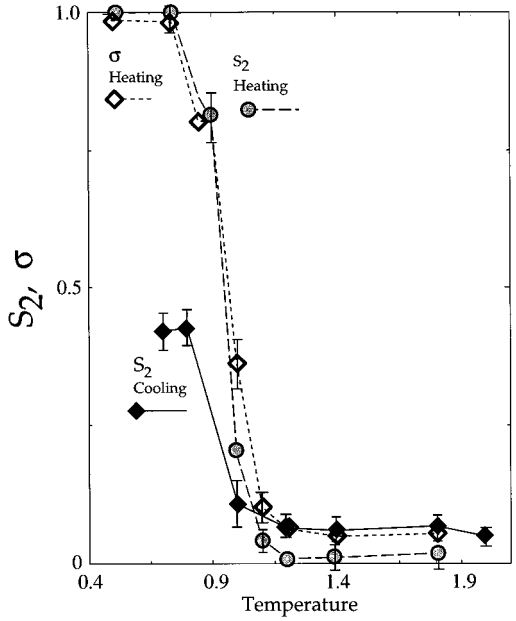

FIG. 3. Orientational order parameter S_2 and positional order parameter σ at different temperatures, for the *3*-4-*3* system, observed in heating and cooling.

$$\theta_{\text{stiff,flex}} = \langle |\theta_a| \rangle_{\text{stiff,flex}} \quad , \qquad \cos\theta_a = \frac{\mathbf{d}_a \cdot \mathbf{d}_{a-1}}{|\mathbf{d}_a| \cdot |\mathbf{d}_{a-1}|} \quad , \tag{10}$$

where $\langle\ \rangle_{\text{stiff}}$ and $\langle\ \rangle_{\text{flex}}$, respectively, denote the averages over all successive segments in stiff and flexible parts. The angles θ_{stiff} and θ_{flex} are the average angles between two successive segments ($\mathbf{d}_a$ and $\mathbf{d}_{a-1}$ are vectors between neighboring beads within chains) in stiff and flexible parts, respectively.

III. RESULTS

Results are presented from the molecular-dynamics computer simulation on monodisperse systems made of 2880 beads forming 288 chains at bead number density 0.8. If we do not explicitly cite the values for the stiff-stiff interaction parameter ϵ_{att}, it is set to $\epsilon_{\text{att}}=1$.

A. Chains with a central stiff and two flexible parts (*3*-4-*3*)

1. Heating

We heated the system using a temperature step of $\Delta T=0.1$ starting at the low-temperature solid phase with preferential axis *z* to the high-temperature isotropic phase. At each temperature step a minimum stabilization time of $t=10^3$ (corresponding to 2×10^5 time steps) has been taken (by increasing near transitions until $t=10^5$). Computation of order parameters S_2 and σ at different temperatures (Fig. 3) and associated snapshots (Fig. 4) show that our system presents clearly three different phases.

First, we observe a solid phase for $0\leqslant T\simeq0.75$. The orientational order parameter is equal to $S_2\simeq0.98$ and the positional parameter order $\sigma\simeq1.0$. In this phase, the chains

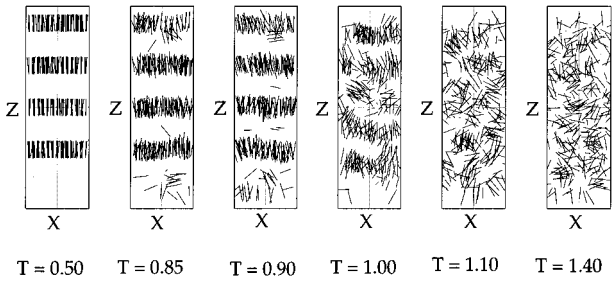

FIG. 4. Snapshots of the stiff part of each molecules projected on the *xz* and *yz* planes at different temperatures (from left to right): $T=0.50$, 0.85, 0.90, 1.00, 1.10, and 1.40 of the *3*-4-*3* system.

remain completely parallel to the initial axis for both flexible and stiff parts. The single-chain static structure factor $S_{\text{SC}}(k_x=0,k_y,k_z)$ displayed in Fig. 5(a) at $T=0.74$ confirms the alignment of the chains. The function S_{SC} is perfectly periodic along the k_z direction with a period equal to the inverse distance between two connected beads and it is practically independent of k_y. A Sm-*A*-like phase occurs between $T\simeq0.75$ and $T\simeq1.2$. The parameters S_2 and σ decrease simultaneously at the clearing point, which is the transition point between the liquid-crystalline phase (nematic or smectic) and the isotropic liquid phase. The parameters S_2 and σ decrease further by increasing the temperature. Within the available precision of the simulated quantities a nematic phase is not seen. At the clearing point, we observe also that the degree of flexibility increases strongly (cf. Fig. 6) in the flexible parts from $\theta_{\text{flex}}\simeq5°$ to $\theta_{\text{flex}}\simeq60°$, while it remains low in the stiff part $\theta_{\text{stiff}}\simeq10°$, independent of temperature. In fact, above the clearing point, the beads in flexible parts become completely free to move and all angles between 0° and ≃120° are possible, which results in an average angle of approximately 60°. Only at low temperature is θ_{stiff} is greater than θ_{flex}, which is surprising. In this regime the disorder in the stiff part could be related to internal low-frequency vibrations due to the rod potential ($U_{\text{FENE}}+U_{\text{LJ}}^{\text{rep}}$) that is used to keep the stiff part stretched. The single-chain static structure factor $S_{\text{SC}}(k_x=0,k_y,k_z)$ at $T=1.0$ is displayed in Fig. 5(b). The function S_{SC} is periodic along a direction slightly different from the direction k_z. For $T>1.2$, finally, we observe a liquidlike phase where S_2 and σ are slightly above zero but not zero. In fact, steric hindrances remain in the system and prevent it from being completely isotropic ($S_2=0$). The radical symmetric single-chain static structure factor $S_{\text{SC}}(k_x=0,k_y,k_z)$ at $T=1.4$ displayed in Fig. 5(d) identifies the isotropic liquid.

2. Cooling

From the configuration of the system at $T\simeq2$ we cooled the sample using a temperature step of $\Delta T\simeq0.1$. The system does not return to a smectic phase with layers normal to the *z* direction (cf. Fig. 4). In fact, as we started by cooling the system from the isotropic phase high above the clearing point, the system lost the global preferential orientation. To obtain global order of the smectic layers one could apply an external electric field that induces a preferential orientation [41]. For $T=0.7$ and $T=0.8$, Fig. 7 shows that the system

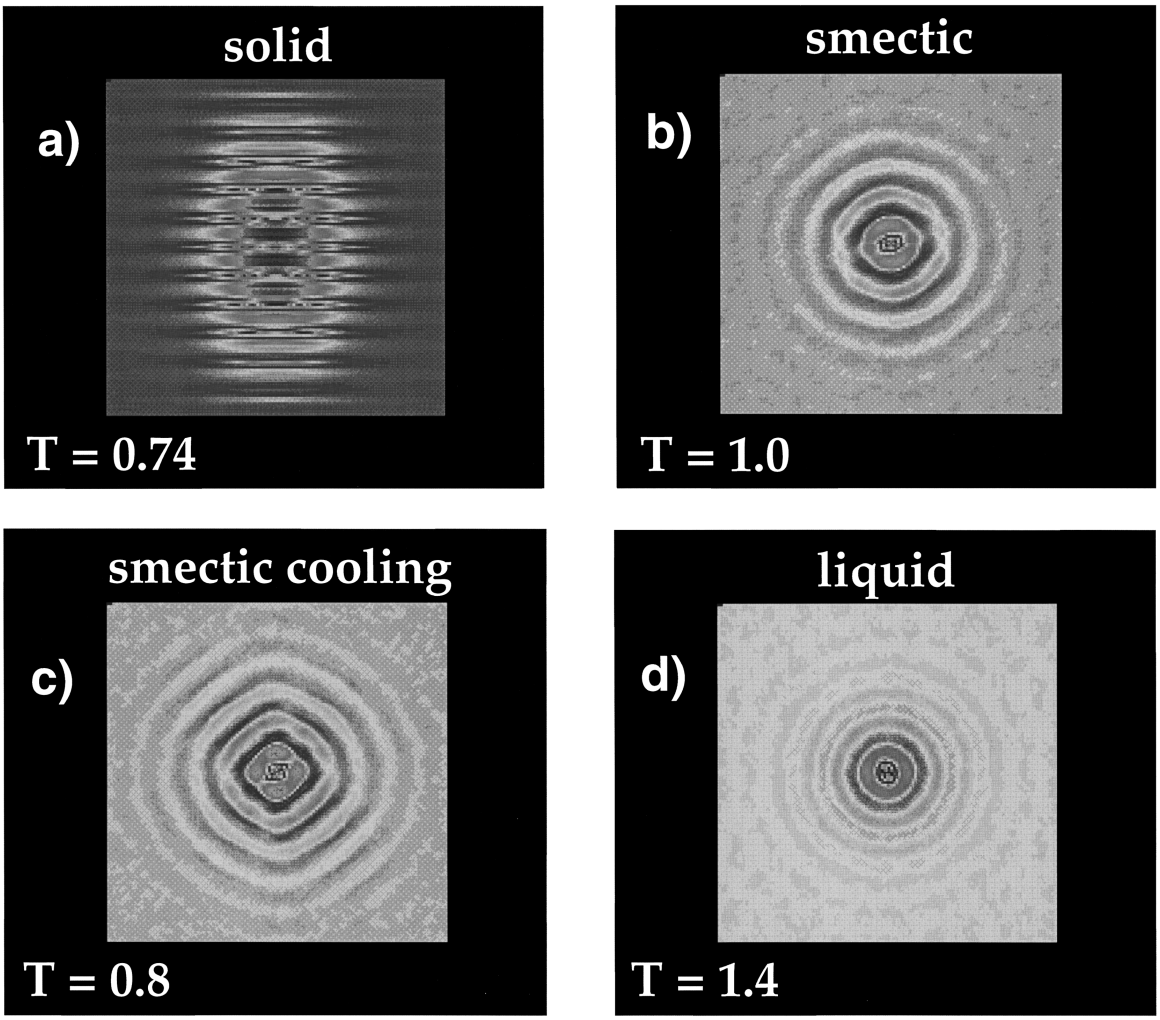

FIG. 5. Single-chain static structure factor S_{SC} as projected onto the x plane ($k_x=0$) at different temperatures (a) $T=0.74$, (b) $T=1.00$, (c) $T=0.80$, and (d) $T=1.40$ for the *3*-4-*3* system.

returns to a smectic phase *locally*, with the appearance of domains where both orientational and positional order are present (two or three layers smectic-*A*-like). Globally, orientational order (cf. Fig. 3) is present. In each domain, the value of the orientational order parameter S_2 is comparable to the values found in heating. However, globally we found a smaller value $S_2 \simeq 0.4$ due the different preferred orientations in the different domains. The single-chain static structure factor $S_{SC}(k_x=0,k_y,k_z)$ at $T=0.8$ [cf. Fig. 5(c)] shows two preferential directions $[011]$ and $[0\bar{1}1]$, unlike the smectic phase observed at $T=1.0$, which are linked with the domains shown in the snapshots of Fig. 4.

3. Pressure and energy

This description of the evolution of the sample as a function of the temperature in three different parts corresponding to the solid, smectic, and isotropic phase is confirmed by the evolution of the pressure tensor and the energy. The contribution to the energy from the stiff-stiff interaction, which is the sum of all the attractive interactions (U_{LJ}^{att}) between the stiff parts, is particularly sensitive to the phase changes and is displayed in Fig. 8. The scalar pressure p is one-third of the trace of the pressure tensor $p=\frac{1}{3}(P_{xx}+P_{yy}+P_{zz})$. The normal pressure difference $p_0=\frac{1}{2}[P_{zz}-\frac{1}{2}(P_{xx}+P_{yy})]$ characterizes an anisotropy of the pressure tensor. The scalar pressure p and the normal pressure difference p_0 are shown in Fig. 9. The normal pressure difference is nonzero in the solid phase. This reflects the extremely anisotropic constraints that keep the chains quasi-perfectly parallel to the z directions, as one can see in Fig. 4. At the transition where the chains become flexible (cf. Fig. 6) p_0 decreases strongly to zero. When heating the sample, the average pressure p and the stiff-stiff energy show a discontinuity that corresponds to the solid-smectic transition. When cooling the system, the curve for the pressure components and the energy also show strong changes at the isotropic-smectic transition. The shear components of the pressure such as $p_+=P_{xy}$ or $p_-=\frac{1}{2}(P_{xx}-P_{yy})$ remain equal to zero at every temperature we simulated.

4. Effects of the attractive interaction

The system presents between $T\simeq 0.75$ and $T\simeq 1.2$ a smectic-*A* phase. The attractive Lennard-Jones potential U_{LJ}^{att} favors the smectic phase as it keeps the molecules par-

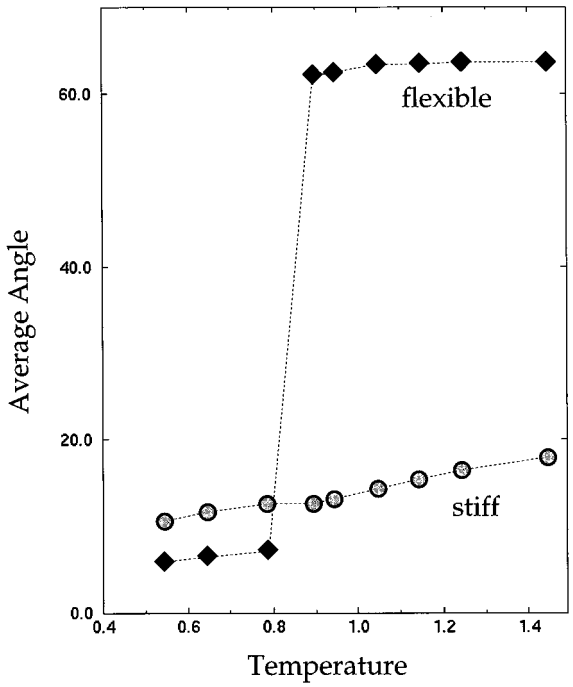

FIG. 6. Angular disorder along the chains in the stiff parts and flexible parts that corresponds to the average angle between two segments defined in Eq. (10), for the *3*-4-*3* system.

allel and in layers. By varying the parameter ϵ_{att}, we investigated the influence of the attractive interaction on the stability of the smectic phase.

The parameter ϵ_{att} has been chosen to be initially fixed at the value $\epsilon_{att}=1$. Figure 10 shows S_2 and σ parameters, both as function of the parameter ϵ_{att}. From a smectic configuration at $T=0.8$, we changed the value of the parameter ϵ_{att} and let the system stabilize at the same temperature. Clearly, we can see that both S_2 and σ parameters are decreasing both to values close above zero. This result shows within the precision of our simulation, that the layers in the sample are less and less well defined but still exist and also that the system does not evolve from the smectic to the nematic phase but directly to the isotropic phase when lowering the

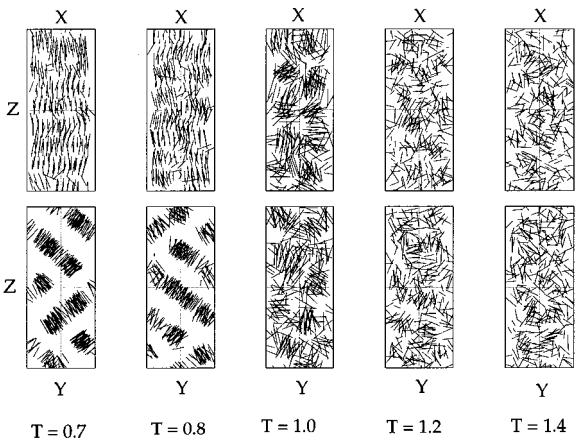

FIG. 7. Snapshots of the stiff part of each molecules projected onto the *xz* and *yz* planes at different temperatures (from left to right): $T=0.70$, 0.80, 1.00, 1.20, and 1.40 for the *3*-4-*3* system.

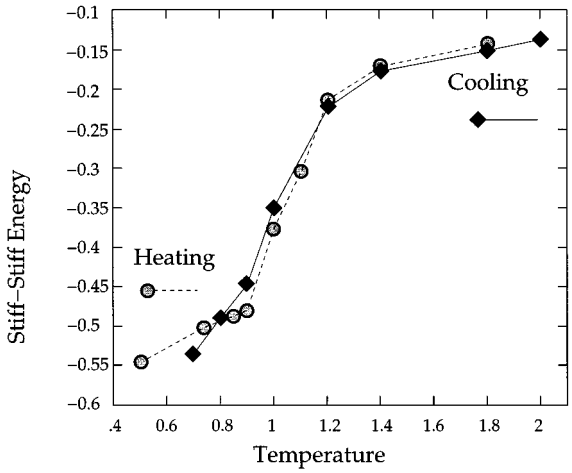

FIG. 8. Stiff-stiff energy, observed in heating and cooling, as a function of the temperature for the *3*-4-*3* system.

attractive interaction parameter.

B. Completely stiff chains (*0*-10-*0*)

1. Heating

It has been observed experimentally that the length of flexible terminals influences the occurrence of smectic and nematic phases [42,43]. In real systems, typically composed of a central aromatic part and two flexible alkyl terminal chains, there exists a strong dispersion interaction between aromatic parts and if flexible terminals are long enough to separate aromatic cores a smectic state can occur [42,43].

For the system studied in [34], no flexible part is present and the smectic phase is almost nonexistent, while the nematic phase is very large. In Sec. III A our system was rather

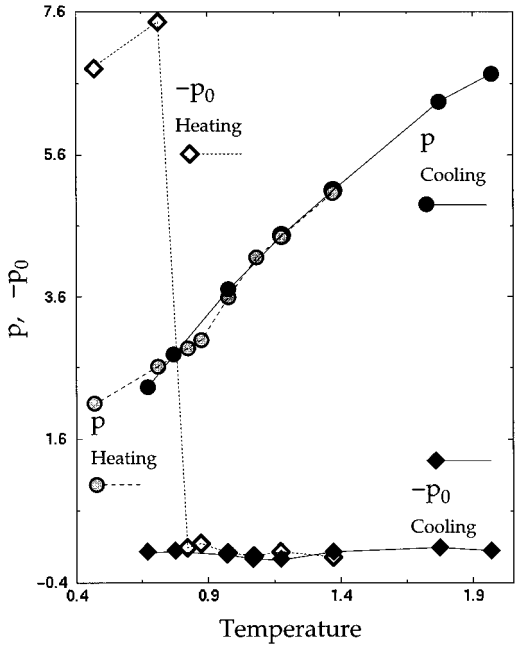

FIG. 9. Scalar pressure p and normal pressure difference $-p_0$ as a function of the temperature in heating and cooling for the *3*-4-*3* system.

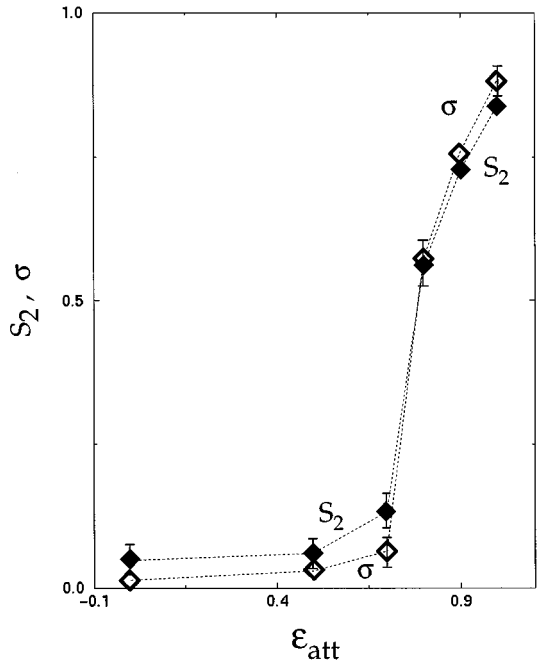

FIG. 10. Order parameters S_2 and σ as a function of ϵ_{att} at the temperature $T=0.8$ for the *3*-4-*3* system.

at the opposite, short stiff part (four beads) and long flexible terminals (six beads): we observed no nematic phase, but a large smectic phase. It is now interesting to study, by decreasing the length of the flexible parts and hence increasing the length of the stiff one in keeping chains with same length, if we do observe a nematic phase. We simulated a set of chains without a flexible part (*0*-10-*0*), which corresponds to the system in [34], but in addition we take into account intramolecular interactions. Figure 11 shows snapshots of the chains projected onto the xy, xz, and yz planes, respectively, at different temperatures. At $T\simeq 3.0$ a transition occurs between the solid phase and a smectic phase, which is a tilted ''pseudohexagonal'' phase. The transition temperature is higher than the transition temperature observed for the system *3*-4-*3*. This increase of transition temperature when the central rigid part length increases has been observed experimentally [42]. The systems order parameter decreases from $S_2\simeq 0.98$ to $S_2\simeq 0.82$. The positional order in the layers can be deduced from the center-of-mass snapshots on xy planes, which present a fcc symmetry in the solid phase (initial configuration) and a hexagonal symmetry above the melting temperature, which becomes more and more disordered when temperature increases.

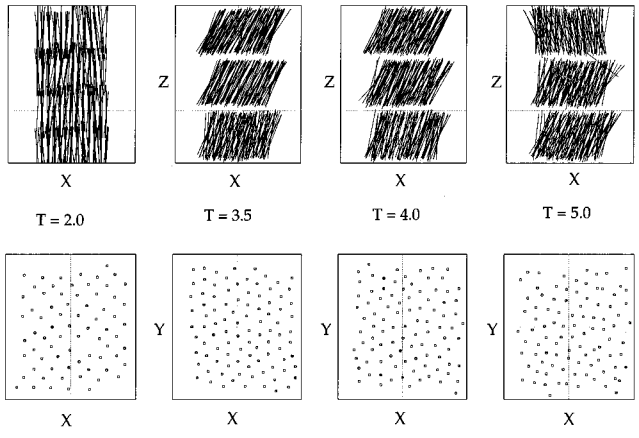

FIG. 11. Snapshots of the stiff part of each molecule projected onto the xz and yz planes at different temperatures (from left to right): $T=2.0$, 3.5, 4.0, and 5.0 for the *0*-10-*0* system.

Above $T\simeq 5$ the chains tend to break due to the kinetic disorder. The study of high temperatures $T>5$ would be required to observe the nematic and isotropic phases. In [34] the clearing point has been observed at $T\simeq 16$. Theoretically the chains are not allowed to break due to the features of intramolecular bond potential (FENE) [see Eq. (3)], but numerically chains can break because of the discrete time step used to integrate the equations of motion. The phenomenon of purposefully breaking the chains for a comparable FENE chain model with a finite depth of the binding potential has been studied recently [44].

2. Effects of attractive interaction (ϵ_{att})

For the *0*-10-*0* system, as for the *3*-4-*3* system, we changed the value of the parameter ϵ_{att} to observe the influence of the attractive potential. At $T=3.00$, $S_2(\epsilon_{\mathrm{att}}=1)\simeq 0.82\pm 0.02$ and $S_2(\epsilon_{\mathrm{att}}=0)\simeq 0.79\pm 0.01$, while $\sigma(\epsilon_{\mathrm{att}}=1)\simeq 0.99$ and $\sigma(\epsilon_{\mathrm{att}}=0)\simeq 0.83\pm 0.03$. As expected, we observe a disordered smectic phase, but no appearance of a nematic phase within the limited range of accessible temperatures.

IV. CONCLUSION

Solid, smectic, and liquid phases have been found in studying a simple microscopic model of thermotropic liquid crystals by molecular-dynamics computer simulations. Symmetric molecules (identical flexible parts) and anisotropic potentials were studied first for semiflexible chains. The model differs considerably from previous models and can be regarded as the most simple approach to model different types of semiflexible chains without introducing nonspherical particles or constraint forces.

All interactions are effectively short ranged and fixed by very few parameters in contradistinction to atomistic simulations for which the research of the potentials itself is part of the work. Due to this feature we obtained very good performance on supercomputers and were able to simulate a large domain of temperatures, which is not the case for the most recent atomistic simulations as cited in the Introduction. Further relevance of the model will have to be shown in comparison with experimental results on chains with well-defined semiflexibility.

From our model for the chain lengths studied here the smectic phase is well defined over a wide range of temperatures, whereas the nematic phase is not present or too narrow in temperature to be seen clearly. The influence of an intermolecular attractive interaction, controlled by the parameter ϵ_{att}, has been analyzed. The smectic phase becomes more and more disordered when the attractive potential decreases, but does not lead to the appearance of a nematic phase.

The influence of the flexibility of the chains has been studied for chain lengths of $n_b\simeq 10$ with different distributions of stiff and flexible parts. Table I shows that there is

TABLE I. Melting and clearing temperature as a function of the ratio r between the stiff length $(n_{\text{stiff}}-1)$ and the chain length n_b.

n_{flex}-n_{stiff}-n_{flex}	$r\equiv(n_{\text{stiff}}-1)/n_b$	Melting temperature	Clearing temperature
3-4-*3*	0.34	0.75	1.2
3-5-*3*	0.40	0.90	2.0
0-10-*0*	1.00	3.0	>5.0

qualitative agreement with experiments for the increase of the clearing temperatures as well as for the melting temperatures when the length of the stiff part increases. This result has been confirmed by additional simulation runs for the system *3*-5-*3* not described in detail in the present paper.

Three conjectures to observe the nematic phase can be made for systems composed of chainlike molecules as considered here. (i) For systems with completely stiff molecules comparable to the system of Paolini *et al.* [34], where the nematic phase is pronounced in a broad temperature regime in contradistinction to the smectic phase, which appears in a small temperature interval, the investigation of our systems at temperatures higher than $T=5$ could be performed with a modification of the rod potential, e.g., by introducing a temperature-dependent depth in order to stabilize the structure of the stiff part [45]. (ii) The system we simulated follows qualitatively the typical experimental phase diagram shown in Fig. 12, where our samples correspond to relatively short chains. Therefore, we can expect to favor a nematic phase if we simulate longer chains $n_b \gg 10$. (iii) As observed experimentally (cf. Fig. 1), nonsymmetric molecules tend to favor the nematic phase. Therefore, simulations for the $(n_{\text{flex}}$-n_{stiff}-$n'_{\text{flex}})$-type molecules, where $n_{\text{flex}}\neq n'_{\text{flex}}$, are desirable.

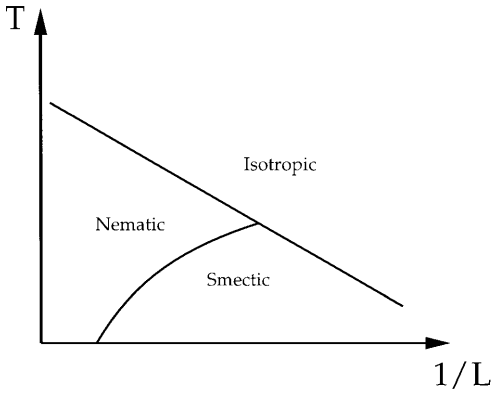

FIG. 12. Typical experimental phase diagram where L is a parameter proportional to the length of the chains as a function of the temperature T [43].

The model and the method presented here can be extended to study nonequilibrium situations, e.g., flow processes. Rheological quantities could be extracted directly from the microscopic knowledge of all bead positions and bead velocities in analogy to previous studies of polymeric model liquids [35,33].

ACKNOWLEDGMENTS

This work has been performed under the auspices of the Sonderforschungsbereich 335: ''Anisotrope Fluide'' of the Deutsche Forschungsgemeinschaft. A.F. thanks the European Communities for financial support via the HCM project ''Development of novel liquid crystal materials.'' We thank the Konrad-Zuse-Zentrum für Informationstechnik (Berlin) for their donation of CPU time on their CRAY Y-MP 4D/464 and T3D supercomputers.

[1] P. G. de Gennes, *The Physics of Liquid Crystals* (Clarendon, Oxford, 1974).
[2] G. Vertogen and W. H. de Jeu, *Thermotropic Liquid Crystals, Fundamentals* (Springer, Berlin, 1988).
[3] S. Chandrasekhar, *Liquid Crystals* (Cambridge University Press, Cambridge, 1971).
[4] N. G. Parsonage and L. A. K. Staveley, *Disorder in Crystals* (Clarendon, Oxford, 1978).
[5] F. Affouard and P. Depondt, J. Phys. (France) I **6**, 98 (1996).
[6] M. P. Allen and M. R. Wilson, Comp. Mol. Design **3**, 335 (1989).
[7] J. P. Bareman, G. Cardini, and M. L. Klein, Phys. Rev. Lett. **60**, 2152 (1988).
[8] S. J. Picken, W. F. Van Gunsteren, P. T. Van Duijnen, and W. H. De Jeu, Liq. Cryst. **6**, 357 (1989).
[9] E. Egberts and H. J. C. Berendsen, J. Chem. Phys. **89**, 3718 (1988).
[10] P. Van Der Ploeg and H. J. C. Berendsen, J. Chem. Phys. **76**, 3271 (1982); Mol. Phys. **49**, 1 (1983).
[11] I. Ono and S. Kondo, Mol. Cryst. Liq. Cryst. Lett. **8**, 69 (1991).
[12] M. E. Mann, C. H. Marshall, and A. D. J. Haymet, Mol. Phys. **66**, 493 (1989).
[13] C. W. Greeff and M. A. Lee, Phys. Rev. **49**, 3225 (1994).
[14] D. Frenkel, Mol. Phys. **60**, 1 (1987).
[15] L. F. Rull, Physica A **80**, 113 (1995).
[16] D. J. Adams, G. R. Luckhurst, and R. W. Phippen, Mol. Phys. **61**, 1575 (1987).
[17] R. R. Netz and A. Nihat Berker, Phys. Rev. Lett. **68**, 333 (1992).
[18] D. Levesque, M. Mazars, and J.-J. Weis, J. Chem. Phys. **103**, 3820 (1995).
[19] A. L. Tsykalo, Mol. Cryst. Liq. Cryst. **129**, 409 (1985).
[20] S. Hess, D. Frenkel, and M. P. Allen, Mol. Phys. **74**, 765 (1991).
[21] M. A. Glaser, R. Malzbender, N. A. Clark, and D. M. Walba, J. Phys. Condens. Matter **6**, A261 (1994); Mol. Simul. **14**, 343 (1995).
[22] R. D. Kamien and G. S. Grest, Condens. Matter **12**, 157 (1995).
[23] E. Paci and M. Marchi, J. Phys. Chem. **100**, 4314 (1996).
[24] M. R. Wilson and M. P. Allen, Mol. Cryst. Liq. Cryst **198**, 465

(1991); Liq. Cryst. **12**, 157 (1992).
[25] C. W. Cross and B. M. Fung, J. Chem. Phys. **101**, 6839 (1994).
[26] A. V. Komolkin, A. Laaksonen, and A. Maliniak, J. Chem. Phys. **101**, 4103 (1994); A. V. Komolkin and A. Maliniak, Mol. Phys. **84**, 1227 (1995).
[27] M. P. Allen, in *Observation, Prediction and Simulation of Phase Transitions on Complex Fluids*, edited by M. Baus, L. F. Rull, and J. P. Ryckaert (Kluwer Academic, Dordrecht, 1995).
[28] H. Heller, M. Schaefer, and K. Schulten, J. Phys. Chem. **97**, 8343 (1993).
[29] D. C. Rapaport, *The Art of Molecular Dynamics Simulation* (Cambridge University Press, Cambridge, 1995).
[30] J. A. Board, J. W. Causey, J. F. Leathrum, A. Windemuth, and K. Schulten, J. Chem. Phys. Lett. **198**, 89 (1992).
[31] A. Windemuth and K. Schulten, Mol. Simul. **5**, 353 (1991).
[32] K. Kremer and G. S. Grest, J. Chem. Phys. **92**, 5057 (1990).
[33] M. Kröger, W. Loose, and S. Hess, J. Rheol. **37**, 1057 (1993).
[34] G. V. Paolini, G. Ciccotti, and M. Ferrario, Mol. Phys. **80**, 297 (1993).
[35] S. Hess, J. Non-Newt. Fluid. Mech. **33**, 305 (1987).
[36] M. P. Allen and D. J. Tildesley, *Computer Simulations of Liquids* (Oxford Science, Oxford, 1990).
[37] L. Verlet, Phys. Rev. **159**, 98 (1967).
[38] K. Kremer, G. S. Grest, and I. Carmesin, Phys. Rev. Lett. **61**, 566 (1988).
[39] H. R. Warner, Ind. Eng. Chem. Fund. **11**, 379 (1972).
[40] C. Zannoni, *The Molecular Physics of Liquid Crystals* (Academic, New York, 1979).
[41] M. Eich, K. Ullrich, and J. H. Wendorff, Prog. Colloid. Polym. Sci. **69**, 94 (1984).
[42] H. Stegemeyer, *Liquids Crystals* (Springer, Berlin, 1994).
[43] A. L. Tsykalo, *Thermophysical Properties of Liquid Crystals* (Golden and Breach, New York, 1991).
[44] M. Kröger and R. Makhloufi, Phys. Rev. E **53**, 2531 (1996).
[45] G. S. Grest and M. Murat, Macromolecules **26**, 3108 (1993).